Estimating the timing of multiple admixture pulses during local ancestry inference

Paloma Medina[*], **Bryan Thornlow**[*], **Rasmus Nielsen**[†] **and Russell Corbett-Detig**[*,1]

[*]Department of Biomolecular Engineering, [1]Genomics Institute, UC Santa Cruz, Santa Cruz, CA 95064, [†]Department of Integrative Biology, UC Berkeley, Berkeley, CA 94720

ABSTRACT Admixture, the mixing of genetically distinct populations, is increasingly recognized as a fundamental biological process. One major goal of admixture analyses is to estimate the timing of admixture events. Whereas most methods today can only detect the most recent admixture event, here we present coalescent theory and associated software that can be used to estimate the timing of multiple admixture events in an admixed population. We extensively validate this approach and evaluate the conditions under which it can succesfully distinguish one from two-pulse admixture models. We apply our approach to real and simulated data of *Drosophila melanogaster*. We find evidence of a single very recent pulse of cosmopolitan ancestry contributing to African populations as well as evidence for more ancient admixture among genetically differentiated populations in sub-Saharan Africa. These results suggest our method can quantify complex admixture histories involving genetic material introduced by multiple discrete admixture pulses. The new method facilitates the exploration of admixture and its contribution to adaptation, ecological divergence, and speciation.

KEYWORDS admixture; *Drosophila melanogaster*; local ancestry inference

Introduction

There is an increasing appreciation for the importance of admixture, an evolutionary process wherein genetically divergent populations encounter each other and hybridize. Admixture has shaped genetic variation within natural plant, animal, and human populations (Pool *et al.* 2012; Rieseberg *et al.* 2003; Hufford *et al.* 2013; Sankararaman *et al.* 2014). If an admixture event has occurred relatively recently, we can use local ancestry inference methods (LAI) to trace the ancestry of discrete genomic segments, called 'ancestry tracts,' back to the ancestral populations from which they are derived (Sankararaman *et al.* 2012; Corbett-Detig and Nielsen 2017; Maples *et al.* 2013; Pool and Nielsen 2009; Price *et al.* 2009). Due to ongoing recombination within admixed populations, the lengths of these ancestry tracts are expected to be inversely related to the timing of admixture. Therefore, it is possible to estimate the timing of admixture events by inferring ancestry tract lengths (Pool and Nielsen 2009; Gravel 2012), or by evaluating the rate of decay of linkage disequilibrium (LD) among ancestry informative alleles (Moorjani *et al.* 2011; Loh *et al.* 2013).

The latter approach is based on modeling expected decay of LD among alleles that are differentiated between admixed populations. Briefly, even if there is little LD in the ancestral populations themselves, admixture will create admixture LD (ALD) within the admixed population among alleles whose frequencies are differentiated between ancestral populations (Chakraborty and Weiss 1988). The decay of ALD is expected to be approximately exponential with a rate parameter that is proportional to the timing of admixture. Two popular methods using this approach, ROLLOFF (Moorjani *et al.* 2011) and ALDER (Loh *et al.* 2013), model the decay of two-locus ALD. However, these methods are limited to estimating the timing of only the most recent admixture event and of only a single admixture pulse. Admixture histories may be more complex, including multiple distinct admixture events (Gravel *et al.* 2013) and multiple ancestral populations (Paşaniuc *et al.* 2009), suggesting that these methods may not be suitable for deeply characterizing the admixture history of many admixed populations (Figure 1). Although, recent work by Pickrell *et al.* (2014) suggests it is possible to detect multiple admixture pulses by modeling LD decay as a mixture of two exponential distributions. Additionally, it may be possible to extend LD decay approaches using three-point linkage disequilibrium to estimate the timing of two admixture pulses in populations with more complex admixture histories (Liang and Nielsen 2016).

A second set of approaches uses the lengths of LA tracts across the genomes of admixed individuals to estimate the timing of admixture events (Gravel 2012; Gravel *et al.* 2013; Pool and Nielsen 2009). Here, the complexity of admixture models that can be accommodated depends on the accuracy of the estimated ancestry tract length distributions within an admixed population. However, these methods require LAI performed prior to estimating population admixture models. LAI necessitates *a priori* assumptions about the admixture model itself, as such assumptions are a prerequisite—implicitly or explicitly—for most LAI frameworks that have been developed to date. These assumptions have the potential to bias the outcomes of LAI and can affect admixture model selection (Pool *et al.* 2012; Sankararaman *et al.* 2008; Corbett-Detig and Nielsen 2017). Additionally, LAI methods require accurately phased

chromosomes—an unlikely prospect for species with low levels of LD (Bukowicki *et al.* 2016) and for relatively ancient admixture events where the rate of phasing switch errors would be similar to the rate of transitions between ancestry types. Therefore, it is often preferable to estimate the timing of admixture events and the LA of a sample simultaneously (Corbett-Detig and Nielsen 2017). Finally, modern sequencing techniques often sequence to light coverage, thus, necessitates a tool that can accommodate read pileup data rather than genotypes.
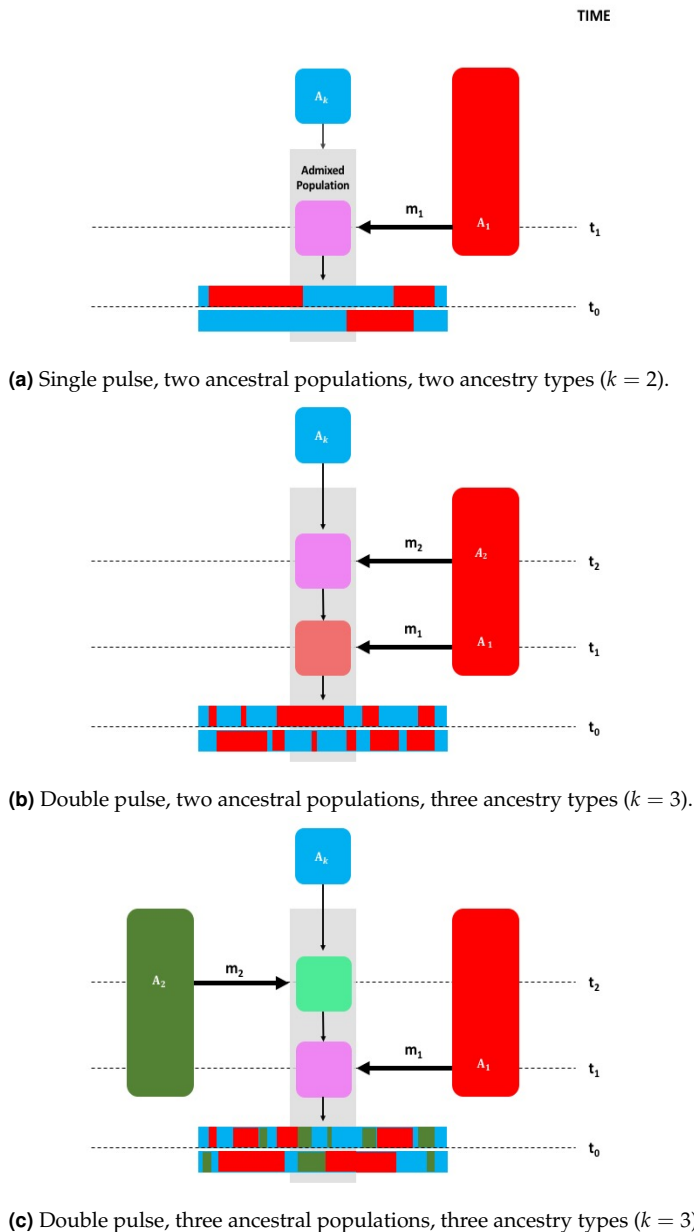

(a) Single pulse, two ancestral populations, two ancestry types ($k = 2$).

(b) Double pulse, two ancestral populations, three ancestry types ($k = 3$).

(c) Double pulse, three ancestral populations, three ancestry types ($k = 3$).

Figure 1 A schematic of (a) a single pulse model with two ancestry types, (b) a two pulse model with two ancestral populations, and (c) a two pulse model with three ancestral populations. A_k is considered the ancestry type of the resident population and would be A_2 in (a) and A_3 in (b) and (c). Note that A_1 and A_2 may come from the same ancestral population, but are modeled as independent states. The gray shaded region draws attention to the admixed population(s). Time since admixture pulses are measured in generations and are denoted as t_1 and t_2, where t_1 occurs more recently than t_2. The time of sampling is represented by t_0, where $t_0 = 0$ if sampling occurred in the present. The proportion of ancestry in the admixed population that entered during an admixture pulse is denoted as m_1 and m_2. Colors represent genetically distinct ancestry types. Local ancestry across a chromosome after admixture is represented by horizontal bars at the bottom of each subplot.

Prior to this study, we developed a framework for simultaneously estimating admixture times and LA across the genomes of admixed populations (Corbett-Detig and Nielsen 2017). Our method can estimate LA and admixture times in a hidden Markov model (HMM) framework assuming a single admixture pulse model. Here, we extend this method to admixed populations that have

experienced multiple ancestry pulses in their recent evolutionary past (Figure 1). We evaluate the performance of this approach using extensive forward-in-time admixture simulations. Finally, we apply this method to study admixed *Drosophila melanogaster* populations in sub-Saharan Africa, and we find evidence consistent with a recent single pulse of cosmopolitan admixture into African populations as well as evidence for more ancient admixture amongst genetically differentiated populations in sub-Saharan Africa.

Model

Overview

In our previous work, we developed an HMM approach to simultaneously estimate local ancestry and admixture times using next generation sequencing data in samples of arbitrary sample ploidy. No phasing is necessary, and unlike most LAI methods, this method models read pileups, rather than genotypes, making this approach appropriate for low coverage sequencing data (Skotte *et al.* 2013). Additionally, although not addressed in this work, our method accommodates samples of arbitrary ploidy, making it ideal for poolseq applications or for populations with unusual ploidy, e.g. tetraploids. Our previous work assumed a single exponential tract length distribution and is therefore limited to accommodating only a single admixture event between two populations (Corbett-Detig and Nielsen 2017). Here, we seek to extend this framework to accommodate additional admixture pulses either from distinct ancestry types or multiple pulses from the same type. Wherever possible, we have kept our notation identical to our previous work to facilitate comparisons between the models.

Implementation and Availability

We implemented the following model into our software package called *Ancestry_HMM* (www.github.com/russcd/Ancestry_HMM). Below, wherever possible, we give the script name and line number responsible for a computation, denoted as *header* : *line_number*. All code is in the *src/* directory within the *Ancestry_HMM* repository.

State Space

Our model incorporates the ancestry of samples with arbitrary ploidy of n chromosomes and with k distinct ancestry types resulting from $k-1$ admixture pulses. Therefore the state space S, is defined as the set of all possible k-tuples of non-negative integers, $H = (l_1, \ldots, l_k)$, such that $\sum_{i=1}^{k} l_i = n$, where l_j is the number of chromosomes in the sample from admixture pulse j.

Emission Probabilities

We model the probability of read pileup data (or alternatively genotypes) of each sample as a function of the allele counts in each ancestral population and assume a uniform prior on the allele frequencies in each source population. Note that where the same ancestral population contributes multiple pulses, the emission probabilities for each site at these states are identical and computed based on the sum of the number of chromosomes of each ancestry type. To accommodate up to k distinct ancestry types, we use multinomial read sampling probabilities. Specifically, if the representation in the read data is exactly equal (in expectation) for each chromosome, the probability of sampling a given read from chromosomes of ancestry pulse k is l_k/n. Therefore, the probability of any given vector of read counts, $R = (r_1, \ldots, r_k)$, sampled from a site with depth r and across the chromosomes in a given hidden state $H \in S$, assuming no mapping or sequencing biases is (*read_emissions.h* : 31)

$$R|H, n, r \sim Mult\left(r, \pi = \left(\frac{l_1}{n}, \ldots, \frac{l_k}{n}\right)\right) \tag{1}$$

Conditional on the read count vector, R, the number of reads carrying the A allele (assuming an A/a di-allelic locus) is independent among ancestry pulses.

For each reference population, the allele count is binomially distributed given the (unknown) true allele frequencies, $f_j, j = 1 \ldots k$. Let C_j represent the total allele count for reference population j and let C_{jA} represent the total number of A alleles for reference population j. Then (*read_emissions.h* : 51),

$$C_{jA}|C_j, f_j \sim Bin(C_j, f_j) \tag{2}$$

While we assume genotypic data for the reference populations, we assume short read pileup data for the admixed population. The (unobserved) allele counts in the admixed chromosomes, stratified by admixture pulse origin, $C_{M1A}, C_{M2A}, \ldots C_{MkA}$ and $C_{M1a}, C_{M2a}, \ldots C_{Mka}$ are also binomially distributed, i.e. for each ancestry type (*read_emissions.h* : 47),

$$C_{MjA}|H, f_j \sim Bin(l_j, f_j) \tag{3}$$

Then, assuming a symmetrical and identical error rate among alleles, ϵ, the probability of obtaining r_{jA} reads of allele A from within the r_j reads derived from chromosomes of type j is (*read_emissions.h* : 47),

$$r_{jA}|H, r_j, C_{MjA}, \epsilon \sim Bin(r_j, (1-\epsilon)\frac{C_{MjA}}{l_j} + \epsilon(1 - \frac{C_{MjA}}{l_j})) \tag{4}$$

By integrating across all possible allele frequencies in the ancestral population assuming a uniform $(0, 1)$ prior, we obtain the probability of a given number of reads of allele A, r_{jA}

$$Pr(r_{jA}|r_j, H, \epsilon) = \sum_{k=0}^{l_k} Pr(r_{jA}|H, r_j, C_{MjA} = k, \epsilon) \int_0^1 Pr(C_{MjA} = k|H, f_j)df_j \tag{5}$$

We then find all possible ways of arranging r_A reads of allele A across the read vector R, $R_A = \{(r_{1A}, \ldots, r_{kA})\}$. Here, for each ancestry type, we require that $0 \leq r_{jA} \leq r_j$ and $\sum_{j=1}^{k} r_{jA} = r_A$. The probability of a given configuration is ($distribute\_alleles.h : 31$),

$$Pr(R_A = R_A^*|R) = \frac{\prod_{j=1}^{k} \binom{r_j^*}{r_{jA}^*}}{\sum_{R_A \in \Omega_R} \prod_{i=j}^{k} \binom{r_j}{r_{jA}}} \tag{6}$$

where Ω_R is the set of all configurations of R_A compatible with R. For each configuration of reads, R and R_A, these above probabilities for each ancestral population combine multiplicatively across all ancestral populations, and we are then able to obtain the emissions probabilities for the hidden state, $H = i$, as

$$Pr(X, C_{1A}, \ldots, C_{kA}|H, \epsilon, n, C_1, \ldots, C_k) = \left(\prod_{j=1}^{k} Pr(C_{jA}|C_j) \right) \sum_{\{R, R_A\} \in \Omega_x} Pr(R_A|R)Pr(R|H, n, r) \prod_{j=1}^{k} Pr(r_{jA}|r_j, n, H, \epsilon) \tag{7}$$

where X is all the read data for the admixed population for the site and Ω_x indicates the set of all values of $\{R_A, R\}$ compatible with X.

Transition Probabilities

Transition probabilities must also be significantly expanded to accommodate the more complicated ancestry models investigated in this work.

Modeling multiple pulses into a single recipient population

First, we consider a scenario where two ancestry pulses enter the same admixed populations at two distinct times (Figure 1c). Here, we will refer to the time of each ancestry pulse as t_k where $t_0 = 0$ and refers to the present and t_1, for example, refers to the most recent admixture pulse in backwards time. During each pulse, a proportion of the resident population, m_k, is replaced. In this model, there are two distinct epochs during which a recombination event may occur along a chromosome. The last epoch, in backwards time, occurs during the time interval between t_1 and t_2. During this time, there are two ancestry types present and the transition rate between them are identical as in our previous work (Corbett-Detig and Nielsen 2017). Specifically, the transition rate between the resident ancestry type A_3 and ancestry type A_2 is

$$2N(1 - e^{\frac{t_1 - t_2}{2N}})m_2 \tag{8}$$

in units of Morgans per segment (Liang and Nielsen 2014). A nearly identical relationship holds for the transition rate from ancestry type A_2 to A_3,

$$2N(1 - e^{\frac{t_1 - t_2}{2N}})(1 - m_2) \tag{9}$$

However, after the second ancestry pulse in forward time, additional transitions between ancestry types A_3 and A_2 will occur. During this interval, the transition rate from ancestry type A_3 to ancestry type A_2 is

$$2N(1 - e^{\frac{-t_1}{2N}})e^{\frac{t_1 - t_2}{2N}}(1 - m_1)m_2 \tag{10}$$

This transition rate reflects the chance of a recombination event occurring between t_1 and the time of sampling with no back coalescence to the previous marginal genealogy in either time epoch. Finally, $1 - m_1$ is the probability that this recombination event does not choose a lineage that entered the population during the second ancestry pulse in forward time, and m_2 is the probability of recombining with a lineage from the first ancestry pulse in forward time. Hence, the total rate of transition between ancestry type A_3 and ancestry type A_2 across both epochs, is

$$\lambda_{32} = 2N(1 - e^{\frac{t_1 - t_2}{2N}})m_2 + 2N(1 - e^{\frac{-t_1}{2N}})e^{\frac{t_1 - t_2}{2N}}(1 - m_1)m_2 \tag{11}$$

Again, a similar rate holds for transitions between ancestry types A_2 and A_3. Transition rates associated with the second ancestry pulse are simpler, and closely resemble those for a single pulse model. Specifically, the rate of transition from ancestry type A_3 to ancestry type A_1 is

$$\lambda_{31} = 2N(1 - e^{\frac{-t_1}{2N}})m_1 \tag{12}$$

Here, we include the probability that a recombination event occurs within the second epoch and that the lineage selects ancestry type A_1. Note that if the lineage selects ancestry type A_1, we need not consider the probability of back coalescence in the time interval

between t_1 and t_2 as it must exit the admixed population during the first ancestry pulse. Similarly, the transition rate from ancestry type A_1 to ancestry type A_3 is

$$\lambda_{13} = 2N(1 - e^{\frac{-t_1}{2N}})(1 - m_1)(1 - m_2) \tag{13}$$

where this equation reflects the probability that a recombination event occurs during the second epoch and then the lineage selects ancestry type A_3. Note that no consideration is given to back coalescence to the previous marginal genealogy during the epoch between t_2 and t_1 because there is no ancestry type A_1 present in the population during this time. Here again, similar rates hold for transitions from ancestry type A_1 to ancestry type A_2 and from ancestry type A_2 to ancestry type A_1 following similar logic presented above.

Transition rates can be generalized to include an arbitrarily large number of distinct ancestry pulses. Briefly, transitions between ancestry types may occur during any epoch in which they are both present within the admixed population. For example, for the first pulse in forward time, transitions between ancestry type A_k and A_{k-1} may occur anytime between t_{k-1} and the present. Therefore, all epochs will be necessarily included the transition calculations between ancestry type A_k and A_{k-1}. More generally, the transition rate between ancestry pulses, i and j, where $1 \leq i < j \leq k$ is,

$$\lambda_{ij} = 2Nm_j \Big(\prod_{l=i}^{j-1} 1 - m_l \Big) \left(1 - e^{\frac{t_{i-1}-t_i}{2N}} + \sum_{q=1}^{i-1} \left(\left(1 - e^{\frac{t_{q-1}-t_q}{2N}} \right) \prod_{p=q+1}^{i} e^{\frac{t_{p-1}-t_p}{2N}} (1 - m_{p-1}) \right) \right) \tag{14}$$

Conversely, if $1 \leq j < i \leq k$, the transition rate between ancestry of pulse i to pulse j is very similar, i.e., transitions may occur during the same epochs (t_j through the present). Therefore,

$$\lambda_{ij} = 2Nm_j \left(1 - e^{\frac{t_{j-1}-t_j}{2N}} + \sum_{q=1}^{j-1} \left(\left(1 - e^{\frac{t_{q-1}-t_q}{2N}} \right) \prod_{p=q+1}^{j} e^{\frac{t_{p-1}-t_p}{2N}} (1 - m_{p+1}) \right) \right) \tag{15}$$

Note that it is not necessary for each ancestry pulse to be derived from distinct ancestral populations. Indeed, we conceived of this approach as a means of fitting multiple pulse ancestry models. Therefore any number of pulses may be contributed by as few as two ancestral populations. However, in order to model full transition rates, it is necessary to estimate the proportion contributed by each pulse even when they are from the same ancestry type, potentially making multiple pulse ancestry models more challenging to fit than models where each pulse is contributed by a separate subpopulation. More broadly, while this model is quite generalizable, there are limits to what is practical to infer using real datasets (see below).

Transition Rates per Basepair

Equations 14 and 15 model transitions in Morgans per segment between ancestry states. We must therefore convert these expressions into a transition rate per basepair. To do this, we multiply the recombination rate by Morgans/bp using an estimate of the local recombination rate within that segment of the genome, r_{bp}. Therefore, the single chromosome transition matrix, $P(l) = P_{ij}(l), i, j \in S$, for a two pulse population model for two markers at distance l basepairs from one another would be as follows (*create_transition_rates.h* 69).

$$P(l) = \begin{bmatrix} 1 - (\lambda_{12} + \lambda_{13})r_{bp} & \lambda_{12}r_{bp} & \lambda_{13}r_{bp} \\ \lambda_{21}r_{bp} & 1 - (\lambda_{21} + \lambda_{23})r_{bp} & \lambda_{23}r_{bp} \\ \lambda_{31}r_{bp} & \lambda_{32}r_{bp} & 1 - (\lambda_{31} + \lambda_{32})r_{bp} \end{bmatrix}^l \tag{16}$$

Modeling Sample Ploidy

The above model describes the ancestry transitions along a single chromosome. However, many datasets contain samples that are diploid or pooled rather than haploid, or equivalently completely inbred. For simplicity, we model each sample of ploidy n as the union of n independent admixed chromosomes. To approximate the transition probability from state i to state j in a sample of n chromosomes, we assume the ancestry proportion, m, contributed by ancestry type A are known. Let the current hidden state ancestry vector be $s = \{s_1, s_2, ..., s_k\}$ where k is the maximal number of ancestry types and s_i indicates the number of chromosomes with ancestry component i. Then $t = \sum_{i=1}^{k} s_i$ is the total number of different chromosomes in the pool. Furthermore, let $P_{ij}(d)$ be the d-step transition probability from ancestry i to j of the previously defined 1-chromosome process. Define q_{ij} as $q_{ij} = s_i P_{ij}(d)$. Also, let $a = \{a_1, a_2, ..., a_k\}, t = \sum_{i=1}^{k} a_i$, be the ancestry vector d sites downstream from the location of the locus with ancestry vector s. Then, we will approximate the transition probability from, s to a, as

$$p(a|s) = \sum_{z \in Z} \prod_{i=1}^{k} \binom{s_i}{z_{i1}, z_{i2}, \ldots, z_{ik}} \prod_j q_{ij}^{z_{ij}}$$

where $z = \{z_{ij}\}$ is an $k \times k$ matrix of non-negative integers and Z is the set of all such matrices for which $\sum_{i=1}^{k} z_{ij} = a_j \forall a_j \in a$ and $\sum_{i=1}^{k} z_{ji} = s_i \forall s_i \in s$. The sum over all $z \in Z$ can be large and increases exponentially in k.

The true ancestral recombination graph is potentially more complex than our simple approximation which assumes all ancestry transitions to be independent. Therefore, caution is warranted when using our model on samples with higher ploidy (Corbett-Detig and Nielsen 2017) (*transition_information.h* : 21).

5

Model Optimization

Because the search space for admixture models is potentially quite complex, we have implemented optimization using the Nelder-Mead direct search simplex algorithm (Nelder and Mead 1965) to optimize the HMM using the forward-equation to compute model likelihoods. As with all direct search algorithms, there is no guarantee that the optimum discovered is a globally optimal solution. We therefore include random-restarts to insure that the globally optimal solution can be recovered consistently.

Assumptions

Perhaps the central assumption of this approach is that admixture occurs in discrete, distinct "pulses." Whereas this is violated in a wide array of true admixture events with either ongoing or periodic admixture (Pool and Nielsen 2009; Gravel 2012), the pulse model is tractable for estimating admixture histories (Corbett-Detig and Nielsen 2017; Loh *et al.* 2013; Gravel 2012). We have previously shown that LAI using our method is robust to a wide array of perturbations including continuous migration and natural selection (Corbett-Detig and Nielsen 2017). Nonetheless, all results, particularly those that hinge heavily on the precise timing of admixture events, should be interpreted cautiously. See also our discussion below.

Validation

Confirmation of the Ancestry Tract Length Approximation

We first confirmed that our sequential Markov coalescent (SMC') approximation for the ancestry tract length distribution is correct. Specifically, we simulated tract length distributions from the forward-in-time simulation program, SELAM (Corbett-Detig and Jones 2016), and compared those with the expected tract length distribution under our model. In comparing the two, we found that the model provides an excellent approximation for the ancestry tract length distribution (Figure 2). This therefore indicates that our SMC' tract length approximation is likely to be sufficient for our purposes. Moreover, we also confirmed that this framework can also accurately accommodate models involving more ancestral populations (Table S1, Figure S1).
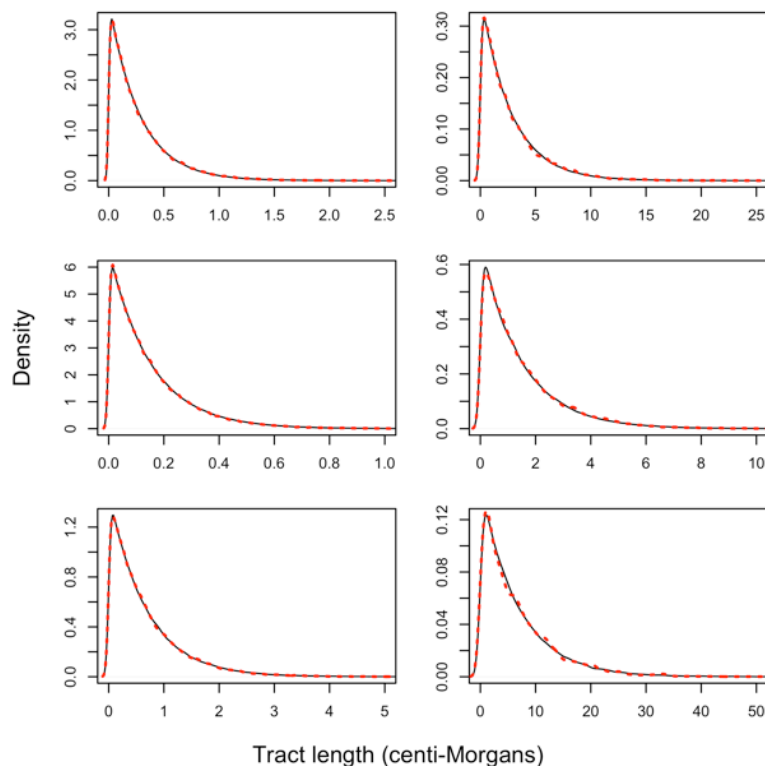

Figure 2 Tract length distributions obtained using our tract length model approximation (solid black) and forward-in-time simulation (dashed red). In the model considered, an initial pulse of ancestry type A_2 entered a resident population of ancestry type A_3 and replaced $\frac{1}{3}$ of the resident population. Then, a second ancestry pulse in forward time, from ancestry type A_1, replaced $\frac{1}{4}$ of the resident population. Each simulation had a diploid population size of size 10,000 and we aggregated data from 50 sampled individuals across 100 simulations to produce the full tract length distribution. From top to bottom, respective ancestry tract length distributions correspond to ancestry type A_3, A_1, and A_2. We investigated two admixture models. The first model has a first and second pulse occurring 200 and 1,000 generations, respectively, before the present (left). The second model has a first and second pulse occurring 20 and 100 generations, respectively, prior to the present (right).

Simulation Ancestral Populations

We used the approach of Corbett-Detig and Nielsen (2017) to validate our HMM software implementation and to test the performance of this expanded model. Briefly, we simulated ancestral genotype data using the coalescent simulation framework MACS (Chen *et al.* 2009), we then simulated ancestry tract length distributions in forward-time using our software package SELAM (Corbett-Detig and Jones 2016). Genotype data for admixed individuals was then drawn from the ancestral data simulated using MACS where genotypes were drawn from each population and assigned to each tract based on that tracts' ancestry type. To explore a wide range of genetic divergences among ancestral populations, we simulated genotype data for ancestral populations at varying levels of genetic divergence from one another. Specifically, we considered populations that are 0.05, 0.1, 0.25, 0.5, and 1 N_e generations divergent from one another.

Linkage Disequilibrium (LD) Pruning

LD among sites may inflate transition rates between ancestry states. In order to mitigate this, we first pruned sites in strong linkage disequilibrium in each reference panel by computing LD among all pairs of markers within 0.1cM of each other. We then discarded one site from each pair with increasingly stringent pruning until we found that admixture time estimates were approximately unbiased in two pulse admixture models. We note that the LD pruning necessary for two pulse models appears to be sufficient for fitting more complex models of admixture (see below). This suggests that simple single-pulse admixture simulations could be used successfully to determine the necessary levels of LD pruning. Also, we found that substantially more stringent LD pruning is necessary to produce unbiased admixture time estimates for ancestral populations that are minimally divergent from one another (Figure S2).

Three Ancestral Populations

We next sought to evaluate the accuracy of this method when two ancestry pulses are contributed from distinct ancestral populations. For all levels of population divergence considered, we find that our method recovers the correct times of admixture events with reasonably high accuracy for recent admixture times (Figure 3). Notably, the error in time estimates decreases substantially with increasingly divergent ancestral populations indicating that this method will produce the most accurate results when ancestral populations are highly genetically divergent.
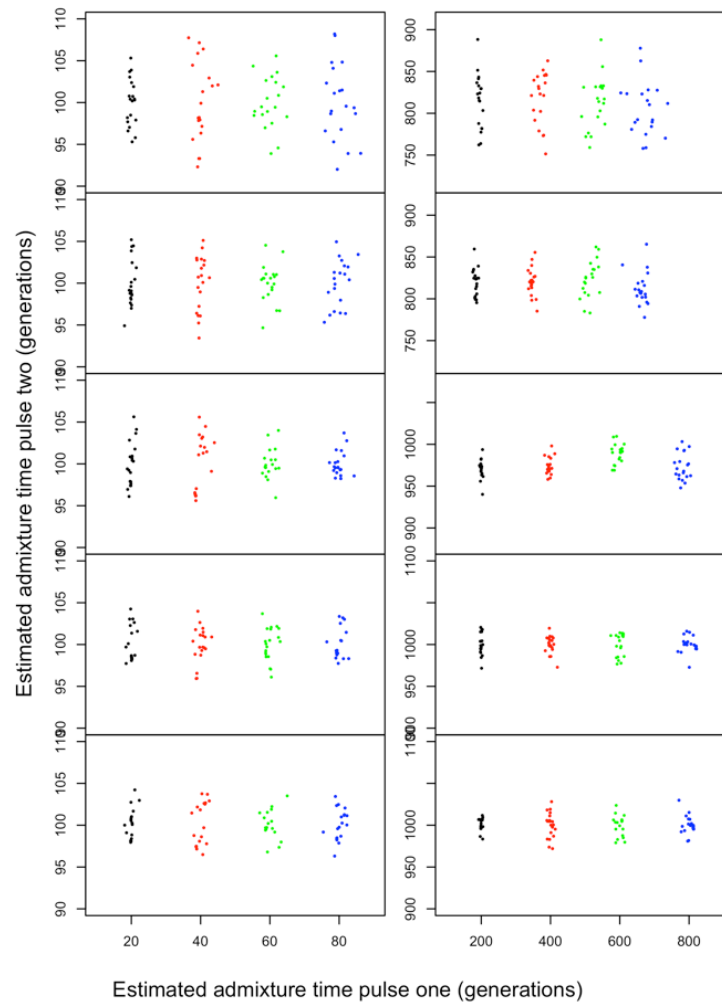
Figure 3 Admixture time estimates for two pulse population models with three distinct ancestral populations. From top to bottom, panels include the divergence time between the ancestral populations is 0.05, 0.1, 0.25, 0.5 and 1 N_e generations. On the left, for all admixture models considered, the second pulse occurred 100 generations before the present. The first pulse occurred 20 (black), 40 (red), 60 (green), and 80 (blue) generations prior to sampling. On the right, the second pulse occurred 1000 generations before the present and the first pulse occurred at 200 (black), 400 (red), 600 (green) and 800 (blue) generations prior to sampling. Note that due to underestimation of admixture times, the figure axes differ between panels for plots of more ancient admixture events.

Whereas our method accurately estimates admixture times when admixture events occur at intermediate times prior to sampling, we find that the accuracy suffers somewhat when estimating the timings of two more ancient admixture events. Indeed, for modestly divergent ancestral populations, e.g., $0.1N_e$ generations divergent, we find that our approach consistently underestimates the times since admixture events, particularly for the more ancient ancestry pulse (Figure 3). This is true despite a nearly linear relationship for estimated admixture times and actual admixture times in a single pulse two ancestral population model (Figure S3), indicating that there is a significant cost for accuracy of model estimation when estimating additional ancestry pulse parameters. However, for more divergent ancestral populations, it is still feasible to obtain accurate admixture time estimates (Figure 3). Additionally, because there is still a monotonic relationship between the time estimates and true admixture times, it might be feasible to correct for this bias and obtain accurate admixture time estimates even when ancestral populations are not particularly divergent.

Two Pulse Admixture Model

It is significantly more challenging to distinguish between models with a single ancestry pulse and models with two distinct ancestry pulses from the same ancestral population. As we described above, one of the key difficulties is that in addition to estimating admixture times, our model must also estimate the proportion of the total ancestry contributed by each pulse. Furthermore, it is essential that this approach includes a mechanism for distinguishing between single and double pulse models. We therefore began with a single-pulse admixture simulation and fit both single and two pulse admixture models to these data.

We find that traditional likelihood ratio tests universally favor two pulse versus single pulse models even when data are simulated under a single pulse model for all scenarios that we considered (Figure S4). We therefore suggest that when using this method to analyze admixed populations, it will usually be preferable to choose the simplest admixture model that is consistent with the data.

More complex models are usually favorable by standard statistical comparisons, but may overfit the data. This consideration is reminiscent of concerns for the STRUCTURE model (Pritchard *et al.* 2000; Evanno *et al.* 2005). In general, this means the model that contains the fewest distinct ancestry pulses should be selected.

Spurious admixture models can be identified by interrogating the timing and proportion of ancestry contributed by each admixture pulse. First, many of the resulting two pulse admixture models contain ancestry pulses with similar times (Figure 4, Tables S2, S3, S4), suggesting that these could be recognized as representing a single admixture event. Second, of the models containing two pulses, many contain one pulse near the correct admixture time and another distant pulse that introduced a very small proportion, i.e. 1% or less, of the total ancestry in the sampled admixed population (Figure 4, Tables S2, S3, S4). Often the pulse introducing a small proportion of ancestry in the sampled population occurred in the distant past, where admixture time is harder to estimate. Therefore, admixture pulses that (1) occur in the distant past and contribute relatively small proportions of the total ancestry or (2) pulse at similar times, may indicate a spurious admixture model and should be disregarded in favor of simpler admixture scenarios.
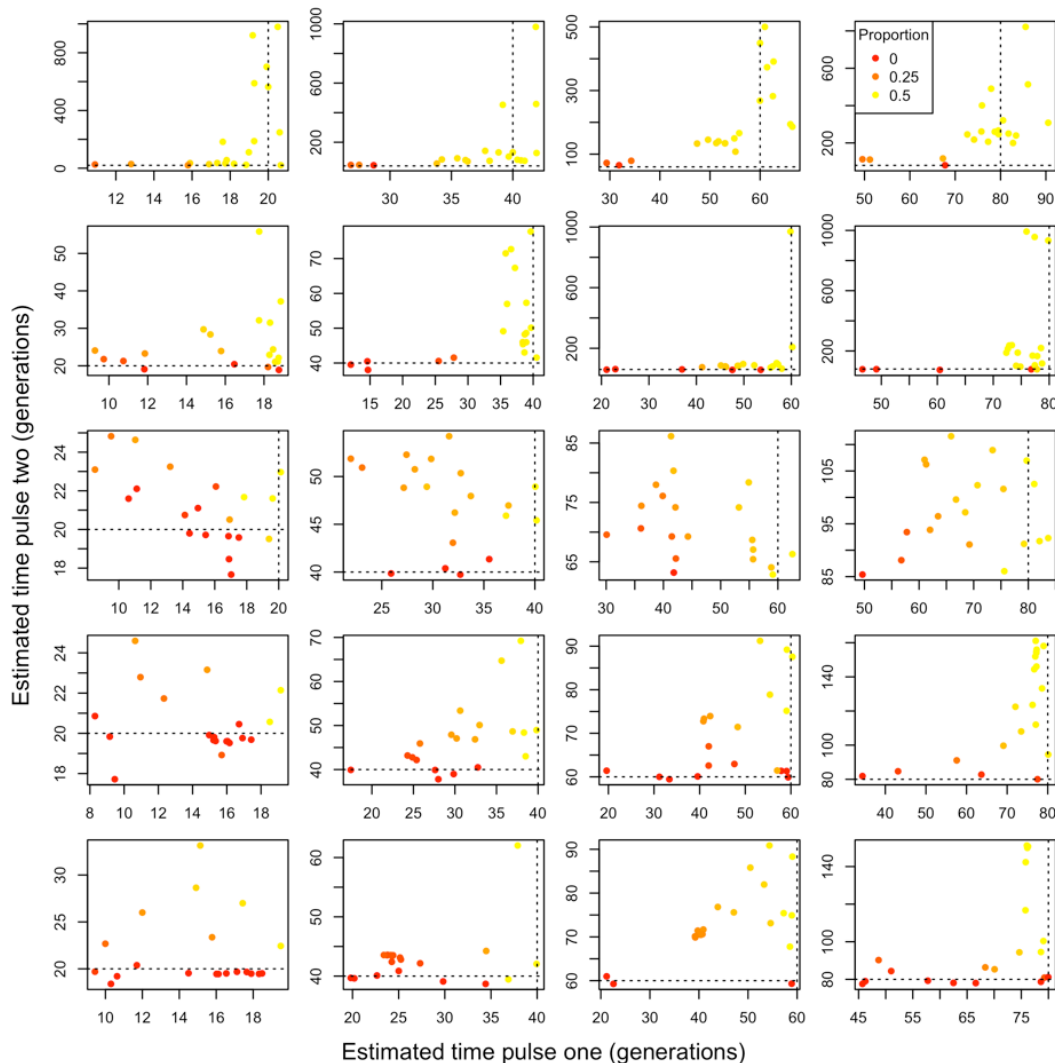

Figure 4 Two-pulse admixture models fitted using our framework to data generated under a single pulse admixture model. We considered varying levels of population divergence. From top to bottom, the ancestral populations are 0.05, 0.1, 0.25, 0.5, and 1 N_e generation divergent from one another. From left to right, the single admixture pulse occurred 20, 40, 60, and 80 generations prior to sampling and replaced one half of the ancestry. Point colors correspond to the proportion of ancestry that is attributable to the second pulse with a gradient running from 0 (red) to the maximum possible, 0.5 (yellow). Dashed lines reflect the true admixture time.

When we simulated admixed populations whose histories contained two distinct ancestry pulses, we found two-pulse models could sometimes be fit accurately. Specifically, when the two ancestry pulses occurred at fairly different times (e.g., 20 and 100 and 200 and 1000 generations), our approach identified models that correspond closely to the parameters under which the admixed population was simulated. However, when the two ancestry pulses occurred at closer time intervals, we were less frequently able to reliably

9

recover the correct admixture model (Figure 5, Figure S3). Additionally, we note that the accuracy of two-pulse models depends on the genetic distance between ancestral populations (Figure 5), where it is generally more straightforward to fit admixture models for genetically distant ancestral populations.
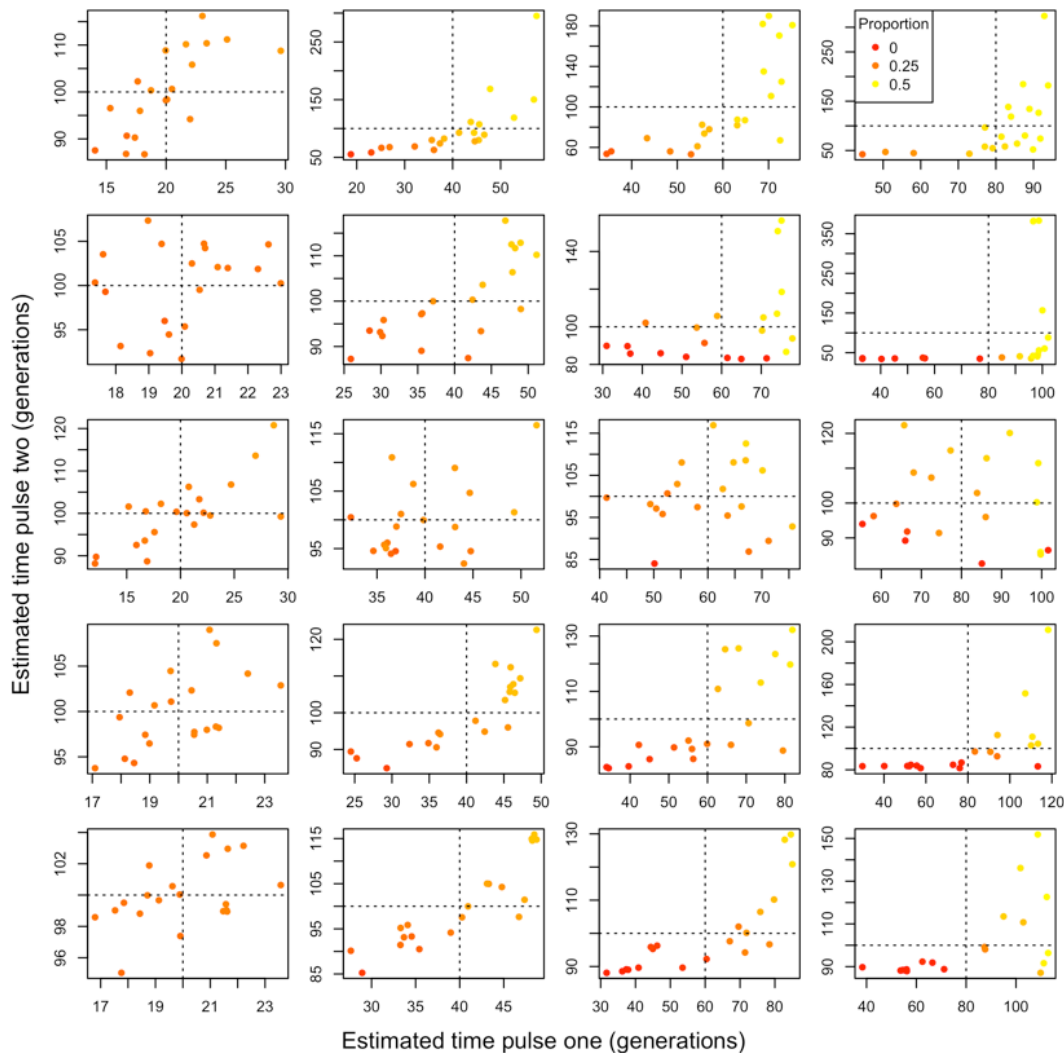

Figure 5 Two-pulse admixture models fitted using our framework to data generated under a two pulse admixture model. We considered varying levels of population divergence. From top to bottom, the ancestral populations are 0.05, 0.1, 0.25, 0.5, and 1 N_e generation divergent from one another. For all models, the second admixture pulse occurred 100 generations prior to sampling. From left to right, the first pulse occurred 20, 40, 60, and 80 generations prior to sampling. The second pulse replaced $\frac{1}{3}$ of the resident population and the first pulse replaced $\frac{1}{4}$ of the resident population. Therefore, each ancestral population contributed one half of the ancestry at the time of sampling. Point colors correspond to the proportion of total ancestry at the time of sampling that is attributable to the first pulse with a gradient running from 0 (red) to the maximum, 0.5 (yellow). Dashed lines reflect the true admixture times for the first and second pulse.

Collectively, our results suggest that it might not be possible to distinguish between single-pulse and two-pulse admixture models when ancestry pulses occurred at similar times. However, it is feasible to distinguish single pulse models from admixture models with both relatively ancient and recent admixture. Therefore, we anticipate that this approach will be valuable for investigating a range of hypotheses with dramatically different admixture times. Furthermore, as we consider here intermediate-sized population samples, i.e. 50 individuals, it may be feasible to distinguish more fine-grained admixture models using larger samples sizes.

LAI Accuracy

We note that while two pulse models do improve the accuracy of LAI, the improvement observed tends to be slight (Tables S2, S3, S4). This suggests that for studies aimed at evaluating patterns of LA across the genome, there may be no need to extensively optimize admixture models to obtain reasonable estimates of the LA landscape in the admixed population. Single pulse models may be sufficient

to accurately characterize LA across the genome for many admixed populations.

Application

Admixture in D. melanogaster

Biogeographical evidence (Lachaise *et al.* 1988) and patterns of genetic variation (Thornton and Andolfatto 2006; Begun and Aquadro 1993; Caracristi and Schlötterer 2003) suggest that *D. melanogaster* originated in sub-Saharan Africa, and went on to colonize much of the rest of the world relatively recently (Duchen *et al.* 2013). During this expansion, the population that left sub-Saharan Africa experienced a dramatic bottleneck that reshaped patterns of genetic diversity across much of the genome (Caracristi and Schlötterer 2003; Ometto *et al.* 2005; Duchen *et al.* 2013). The resulting "cosmopolitan" haplotypes are distinguishable from those of the ancestral sub-Saharan populations based solely on patterns of genetic variation (Pool *et al.* 2012) and these two ancestral populations have since encountered each other and admixed in numerous geographic locations within sub-Saharan Africa and worldwide (Pool *et al.* 2012; Caracristi and Schlötterer 2003)

Thus, *D. melanogaster* has emerged as an important model for understanding the genomic and phenotypic consequences of admixture in natural populations. There are important pre-mating behavioral isolation barriers between cosmopolitan and African individuals (Ting *et al.* 2001), as well as substantial phenotypic consequences that operate post mating within admixed individuals (Lachance and True 2010; Kao *et al.* 2015). Additionally, recent work has investigated the genomic consequences of admixture both demographically (Duchen *et al.* 2013; Bergland *et al.* 2016) and with the goal of evaluating the impact of natural selection in shaping genome-wide patterns of variation (Pool 2015). The genomic consequences of admixture have only been studied using relatively simple demographic models (i.e. a single event, (Pool *et al.* 2012)), leaving open the possibility that more complex admixture dynamics are common in natural populations of this species. Accurately characterizing the admixture histories and the patterns of local ancestry across the genome is essential to further our understanding of the demographic history of this species and build a complete null model for studying natural selection on ancestry during admixture.

Evaluating Possible Applications to D. melanogaster Admixed Populations

In agreement with our general conclusions from admixture simulations, we find that our method is accurate, and single-pulse admixture models are distinguishable from two-pulse models for temporally distinct admixture events (i.e., wherein two pulses occurred at significantly different times, Figure 6). However, also consistent with our results above, we find that when admixture pulses occurred at relatively similar times (e.g. $t_1 = 200$ and $t_2 = 250$ generations prior to sampling), a single ancestry pulse contributes the vast majority of admixed ancestry, and this scenario is therefore ultimately most similar to a single pulse admixture model. These data therefore suggest that it is possible to distinguish single from two pulse admixture models in data consistent with *D. melanogaster* ancestral populations when the admixture pulses occurred at dramatically different times.

Perhaps owing to the higher marker density, the greater accuracy of genotyped markers along the genome, and/or the inbred genomes in our Drosophila samples, we find that our method is slightly more accurate for population histories consistent with those of *D. melanogaster* than for the simulated populations considered above (Tables S2, S3, S4). Additionally, admixture times can be accurately estimated even when admixture events occurred in the distant past (e.g., 5000 generations prior to sampling, Figure 6).
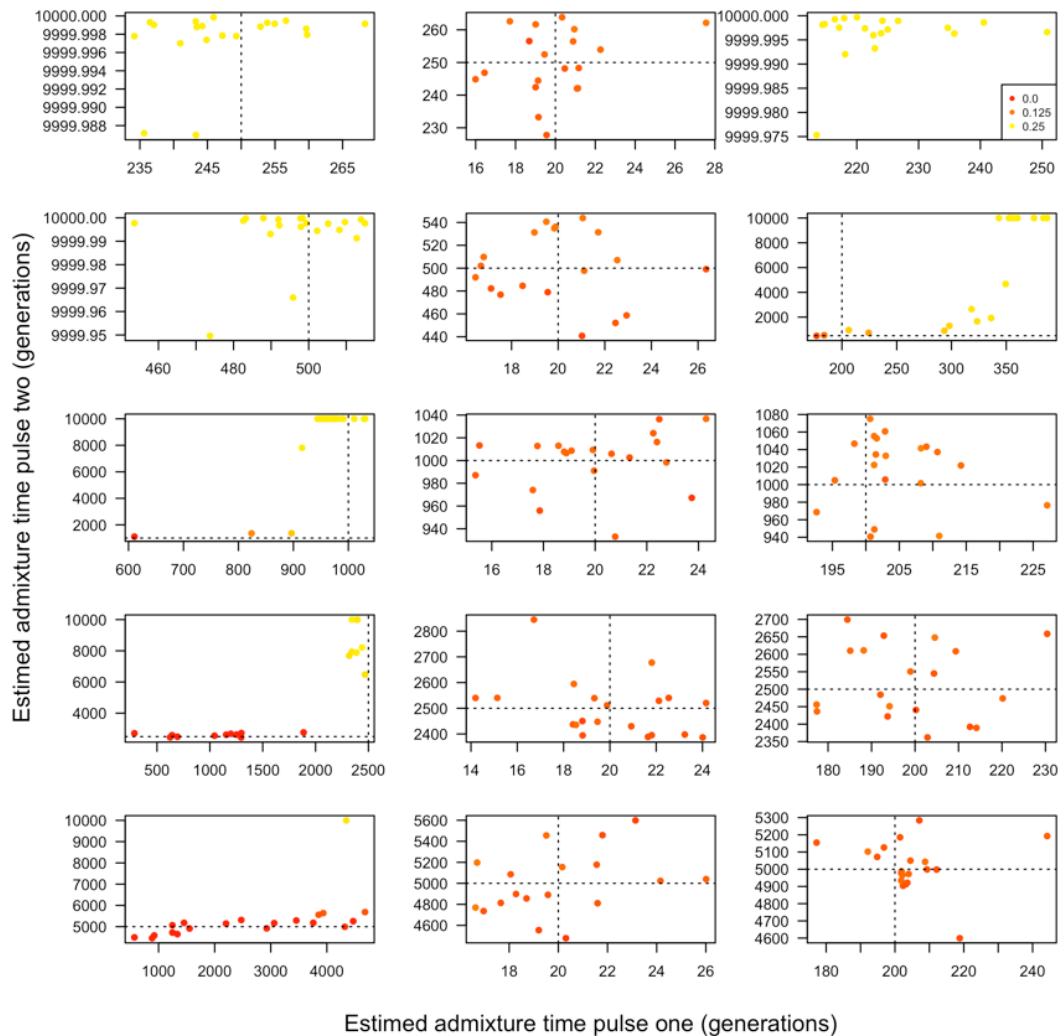
11

Figure 6 Admixture model fitted for data consistent with admixed Drosophila populations. Two-pulse admixture models for scenarios that are truly single-pulse (left), two pulse with a first admixture pulse 20 generations prior to sample (middle), and two pulse models with a first admixture pulse 200 generations prior to sampling (right). From top to bottom, the second admixture pulse occurred 250, 500, 1000, 2500, and 5000 generations prior to sampling. The point colors indicate the proportion of ancestry in the sampled population that entered during the first admixture pulse in backwards time with a gradient running from 0 (red) to the maximum, 0.5 (yellow). Dashed lines indicate the correct timing of simulated ancestry pulses. In two pulse models, the first pulse contained 10% of the final ancestry and the second contributed 14% of ancestry to the sampled population. In single pulse models, all of the non-native ancestry is contributed by one pulse. These values were selected to be consistent with those from admixed sub-Saharan populations of this species (Pool *et al.* 2012). Note that the axes differ significantly across plots.

Application to Admixed D. melanogaster Samples

To demonstrate the performance of our method on real datasets, we applied our approach to *D. melanogaster* variation data from sub-Saharan African populations (Figure 7). We studied populations from Rwanda (RG), South Africa (SD) and Gambella, Ethiopia (EA) and estimated the time of cosmopolitan admixture using both double and single pulse models.

In two pulse models, cosmopolitan ancestry pulsed twice (Figure 1b) and resulted in the most recent pulse contributing approximately 99% and 97.5% (for RG and SD respectively) of the total cosmopolitan ancestry present in the population at the time of sampling. The second, more ancient pulse, tends towards the maximum time allowed in our inference method, 10,000 generations, and contributes 0.01% and 2.5% of the total cosmopolitan ancestry present in the population at the time of sampling RG and SD (Figure 7). As described above, a distant admixture pulse contributing small amounts of ancestry likely indicates a spurious admixture model. Though it is possible that ancient cosmopolitan admixture contributed a small amount to the ancestry of the SD and RG populations, the simplest model, a single pulse model with cosmopolitan ancestry pulsing into African ancestry, provides a reasonable description of the demographic history of RG and SD. The estimated admixture times, 140 and 437 generations in a single pulse model, suggest

that the observed cosmopolitan ancestry has entered these populations exceptionally recently despite earlier contact and extensive commerce among human groups.

To test how our method performs when ancestral populations are omitted, we applied a two pulse model to genotype data from Gambella, Ethiopia (EA) which is believed to have West African, Ethiopian, and cosmopolitan ancestry (Lack *et al.* 2015). Instead of modeling all three ancestral populations, we omitted West African as an ancestral population to mimic a scenario where the ancestral populations of an admixed population have not all been identified. The results of the two ancestral state model estimated an ancient admixture pulse composing 6.5% of the total cosmopolitan ancestry present in the population at the time of sampling (Figure 7). Importantly, we note that 6.5% is substantially more than we found in any of our simulated single-pulse datasets. A second pulse about 200 generations ago contributed 28% of cosmopolitan ancestry. Since this two pulse model did not include ancestry from a West African population, it is likely that our method fit a portion of the allele frequency differentiated between the ancestral populations into the ancient pulse of cosmopolitan ancestry. Thus, a large proportion of ancestry contributed by an ancient admixture pulse might indicate the need to identify additional ancestral populations. A two pulse model including three ancestral populations is therefore more appropriate for studying the admixture history of EA.
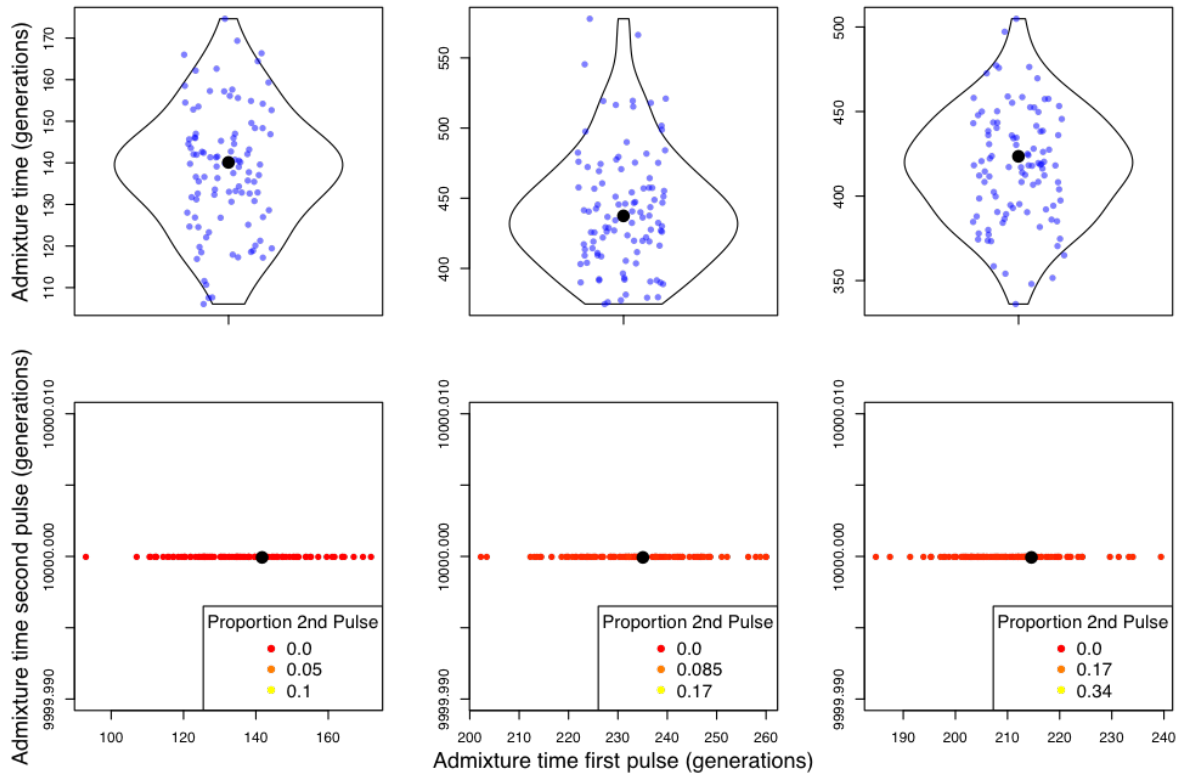

Figure 7 Single and double pulse models applied to real genotype data generated from sub-Saharan African populations of *Drosophila melanogaster*. In the plots shown, cosmopolitan ancestry pulsed into native African ancestry once (top row) or twice (bottom row). The panels from left to right are populations RG, SD, and EA. Single and double pulse models were bootstrapped 100 times. Each point in the top row corresponds to a bootstrap estimate of the timing of admixture. The bottom row shows bootstrap estimates for the timing of the second admixture pulse in backwards time. The point colors indicate the proportion of ancestry in the sampled population that entered during the second (in backwards time) admixture pulse with a gradient running from 0 (red) to the maximum, 0.5 (yellow). Black dots indicate the bootstrapped time optima.

13

Application to Three Population Mixture in Gambella, Ethiopia (EA)

Our results above emphasize the importance of identifying and incorporating variation data from all ancestral populations. Here, we use a two pulse, three ancestral population, admixture model to estimate the order and timing of admixture events into EA (Figure 1c, Figure 8).

The native ancestry of *Drosophila melanogaster* from EA is unknown. Previous studies have suggested both cosmopolitan and sub-Saharan ancestry contribute to the genetic variation in EA (Figure 1c) (Lack *et al.* 2015). To determine the most likely native ancestry of EA, we applied three permutations of a two pulse model to population data from Gambella, Ethiopia. We used unadmixed populations from Ethiopia (EF), cosmopolitan (FR), and West African (AF) to represent ancestral populations of EA and used our program to estimate the timing of admixture in each admixture model. Our three models were: EF and AF pulsing into resident FR ancestry, AF and FR pulsing into EF ancestry, and EF and FR pulsing into AF ancestry.

When FR is supplied as the resident population in the two pulse model, EF and AF both enter the population 1140 generations ago. This is implausible for a variety of reasons. First, even without considering this result, it is unlikely that cosmopolitan ancestry is the native ancestry type in Gambella, Ethiopia. Second, it is exceptionally unlikely that two distinct ancestral populations enter the admixed population at precisely the same time. Finally, the likelihood of the FR native ancestry model is less favored relative to an EF or AF native model by 11000 log likelihood units. We therefore consider a model with native African ancestry, EF or AF, to most likely describe the admixture history of Gambella, Ethiopia *D. melanogaster*.

When EF and AF were modeled as native ancestry, resulting admixture histories were nearly identical, suggesting either EF or AF could be native to Gambella since these are equivalent models. Using a two pulse, three ancestral population model, we estimated the timing of EF and FR admixture pulses in AF native ancestry (Figure 1c). The second pulse in backwards time is estimated to have occurred approximately 4755 generations ago and suggests that EA admixed with genetically distinct sub-Saharan African populations in the relatively distant past (Figure 8). The most recent pulse introduced FR ancestry 355 generations ago, suggesting EA recently admixed with cosmopolitan populations, which is strikingly consistent with our estimates from the other admixed populations in Sub-Saharan Africa (Figure 3, Figure 8). Additionally, the relatively recent admixture between West African and Ethiopian *D. melanogaster*, suggests that Sub-Saharan populations of this species were isolated until very recently (i.e., approximately 338 years ago).

We note that our estimate of admixture time is congruent with an estimate of divergence between Ethiopian and Central African populations. Kern and Hey (2017) estimated Ethiopian and West African *D. melanogaster* diverged approximately 3628 years ago (or approximately 50,000 generations). Our estimates of admixture time occur sufficiently far after this estimated Ethiopian and African divergence time and provide confidence that our three-population admixture model of Gambella (EA) *D. melanogaster* is consistent with previous investigations of demographic patterns of *D. melanogaster* from sub-Saharan African. These data therefore indicate that our approach can successfully estimate the timing of multiple admixture events in the history of a population using real genotype data.
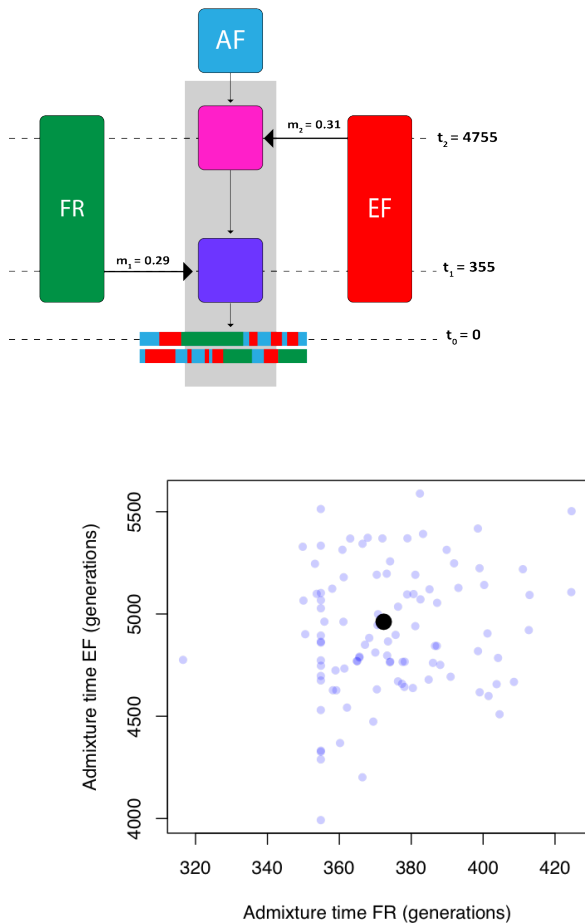
Figure 8 Most likely admixture model fitted to real data generated from Gambella, Ethiopia (EA). Schematic of double pulse admixture model with three ancestral populations and ancestry types is shown (top). 1000 bootstraps were run of FR and EA pulsing into AF native ancestry. Real bootstrap data is shown (bottom), where each point is a bootstrap estimate of FR and EA admixture pulses and the black point represents the optimal admixture model from the full data set.

Conclusion

Admixture histories can be complex with numerous distinct ancestral populations contributing genetic material to a recipient population at multiple times in the past. In this work, we developed coalescent theory as well as a method to estimate the timing of multiple admixture events in an admixed population. We applied our model to forward-time simulated and real sequence data. The results of our simulations suggest that our model can discern between ancestry pulses occurring far apart in time from each other. Moreover, our method excels when the populations contributing ancestry are genetically diverse from each other.

Our approach, when applied to real admixed *Drosophila melanogaster* populations, is consistent with previous results on the African origin and admixture of the *Drosophila melanogaster* species. We find that cosmopolitan ancestry has entered very recently and is best accommodated by our framework using a single pulse model. Additionally, we demonstrate that more complex admixture patterns have shaped the ancestry of Gambella, Ethiopia. We indicate that two ancestry pulses from distinct ancestry types are necessary to explain patterns of genetic variation within this population.

This is the first method that estimates the timing of multiple pulse admixture models while accommodating the possibility of more than one source population. Although not a focus of this study, our method is designed to accommodate read pile-up data, samples of arbitrary ploidy, and samples with unknown admixture history. Taken all together, we anticipate that our approach will facilitate continued exploration of admixture's contributions to fundamental biological processes such as adaptation, ecological divergence and speciation.

Methods

Coalescent Simulations

We simulated ancestral population genetic variation using the coalescent simulation software package MACS (Chen *et al.* 2009). Briefly, to consider a simplified ancestral process, we consider a model where a population, initially of size 2N, subdivided into three daughter populations of identical size, 2N. To assay a range of genetic divergence among the daughter populations, we performed replicate

simulations where we allowed populations to diverge (D in the command line below) for 0.05, 0.1, 0.25, 0.5 and 1 N_e generations. Note that the functionally relevant parameter for LAI using this approach is probably related to allele frequency changes between the ancestral populations, and therefore to the density of ancestry informative markers along the genome, rather than to divergence times per s_e. For example, a population bottleneck would result in rapid and dramatic allele frequency differences despite a short divergence time. Note also that alternative divergence models will also impact the distribution of LD among markers, underscoring the importance of considering each unique model when applying this approach for admixed model estimation.

We therefore used the following command line for all simulated populations:

```
$ macs 600 100000000 -i 1 -h 100 -t 0.001 -r 0.001 -I 3 200 200 200 0 -ej D 2 1 -ej D 3 1
```

This will simulate a single chromosome of length 100Mb with a per-site theta of 0.001 and equal recombination rate. Therefore, these simulations could resemble a reasonably sized mammalian population. This will output 200 chromosomes per ancestral population, and for all admixture simulations, we used the first 100 as the reference panel, and the second 100 to simulation genetic variation across admixed chromosomes.

Admixture Simulations

We simulated admixed populations using the forward-in-time admixture simulation program, SELAM (Corbett-Detig and Jones 2016). We first explored the levels of LD pruning that is necessary for producing unbiased estimates of admixture times using two population, single pulse simulations. All simulations for LD pruning optimizations were run with ancestry proportions 0.5 and 0.5 and with an admixed population size of 5,000 males and 5,000 females.

We then simulated admixture models with three ancestral population models where the resident population contributed $\frac{1}{2}$ of the total ancestry, and each admixture pulse contributed $\frac{1}{4}$th of the total ancestry to the final admixed population. Therefore the first pulse, in forward time, contributed $\frac{1}{3}$ of the admixed population and then had $\frac{1}{4}$th of that ancestry replaced by the subsequent pulse. All simulations were performed across the range of divergence times that we simulated for each ancestral population.

Read Simulation

We simulated short read data for each admixed individual following the approach of (Corbett-Detig and Nielsen 2017). Briefly, reads are drawn binomially from each samples' genotype and read depths from a Poisson distribution with mean equal to 2. That is, we simulated 2X sequencing depths to represent a likely use case of this software where individuals are sequenced to relatively light coverage.

Drosophila Simulation

We have previously used this framework to simulate data consistent with the ancestral populations of *D. melanogaster*, following the coalescent simulation apporach of (Corbett-Detig and Nielsen 2017). All other features of the simulated Drosophila dataset are similar to those above except that we simulated genotypes rather than short read pileup data. We did this because the dataset that we used is sequenced to sufficiently high depths so as to preclude most uncertainty in short read data (Lack *et al.* 2015, 2016).

Drosophila Sample Application

We obtained *Drosophila melanogaster* genotype data for natural isolates from the Drosophila Genome Nexus (Lack *et al.* 2015, 2016), which curates data from more than 1,000 natural isolates of this species. We used the recommended masking packages supplied for that site for all samples in reference populations. For SD, we used the ZI population, for RG we used a set of central and west African samples (as in Corbett-Detig and Nielsen (2017)), and for EA we used the EF population. All cosmopolitan pulses were modeled using FR as the cosmopolitan reference population.

Application to Admixed Samples

We used our model to assay the admixture histories of Rwandan, South African, and Ethiopian samples. We fit both a single pulse model and double pulse model to genotype data from each population, running 100 bootstrap replicates using a block size of 5000 SNPs.

```
- single pulse
./ancestry_hmm -i RG.auto.panel -s RG.ploidy.txt -a 2 0.1 0.9 -p 1 100000 0.9 -p 0 -100 0.1 -g -e 1e-4 -b 100
↪  5000
./ancestry_hmm -i SD.auto.panel -s SD.ploidy.txt -a 2 0.17 0.83 -p 1 100000 0.83 -p 0 -100 0.17 -g -e 1e-4 -b
↪  100 5000
./ancestry_hmm -i EA.auto.panel -s EA.ploidy.txt -a 2 0.34 0.66 -p 1 100000 0.66 -p 0 -100 0.34 -g -e 1e-4 -b
↪  100 5000
- double pulse
./ancestry_hmm -i RG.auto.panel -s RG.ploidy.txt -a 2 0.1 0.9 -p 1 100000 0.9 -p 0 -100 -0.05 -p 0 -100 -0.05
↪  -e 1e-4 -g -b 100 5000
./ancestry_hmm -i SD.auto.panel -s SD.ploidy.txt -a 2 0.17 0.83 -p 1 100000 0.83 -p 0 -100 -0.085 -p 0 -100
↪  -0.085 -e 1e-4 -g -b 100 5000
./ancestry_hmm -i EA.auto.panel -s EA.ploidy.txt -a 2 0.34 0.66 -p 1 100000 0.66 -p 0 -100 -0.17 -p 0 -100
↪  -0.17 -e 1e-4 -g -b 100 5000
```

Application to Three Population Mixture from Gambella, Ethiopia

We used our model to assay the admixture histories of Gambella, Ethiopia. We fit a double pulse model to genotype data from Gambella, running 1000 bootstrap replicates each using a block size of 5000 SNPs. Moreover, since the native ancestry type for Gambella is unknown, we modeled West African (AF), Ethiopian (EA), and French (FR) as the ancestral population.

```
./ancestry_hmm -i three_pop.auto.EA.panel -s three_pop.auto.EA.ploidy -a 3 0.4 0.31 0.29 -p 0 -1000 0.4 -p 1
↪  100000 0.31 -p 2 -1000 0.29 -g -b 1000 5000
./ancestry_hmm -i three_pop.auto.EA.panel -s three_pop.auto.EA.ploidy -a 3 0.4 0.31 0.29 -p 0 100000 0.4 -p 1
↪  -1000 0.31 -p 2 -1000 0.29 -g -b 1000 5000
./ancestry_hmm -i three_pop.auto.EA.panel -s three_pop.auto.EA.ploidy -a 3 0.4 0.31 0.29 -p 0 -1000 0.4 -p 1
↪  -1000 0.31 -p 2 100000 0.29 -b 1000 5000 -g
```

Supplemental

Table S1 Simulated and analytical transition rates for a model with five ancestry types, $k = 5$. t_4, t_3, t_2, t_1, and t_0 are 80, 60, 40, 20, and 0 generations since the present, respectively. m_4, m_3, m_2, and m_1 are $\frac{1}{2}$, $\frac{1}{3}$, $\frac{1}{4}$, and $\frac{1}{5}$ respectively.

From	To	Rate_Simulation	Rate_Analytical
5	4	25.715	25.625
5	3	15.509	15.645
5	2	9.045	8.991
5	1	4.025	3.998
4	5	25.449	25.625
4	3	15.654	15.645
4	2	8.956	8.991
4	1	3.978	3.998
3	5	15.640	15.645
3	4	15.509	15.645
3	2	8.920	8.991
3	1	4.013	3.998
2	5	9.007	8.991
2	4	9.066	8.991
2	3	9.058	8.991
2	1	3.955	3.998
1	5	3.936	3.998
1	4	4.001	3.998
1	3	3.970	3.998
1	2	4.001	3.998
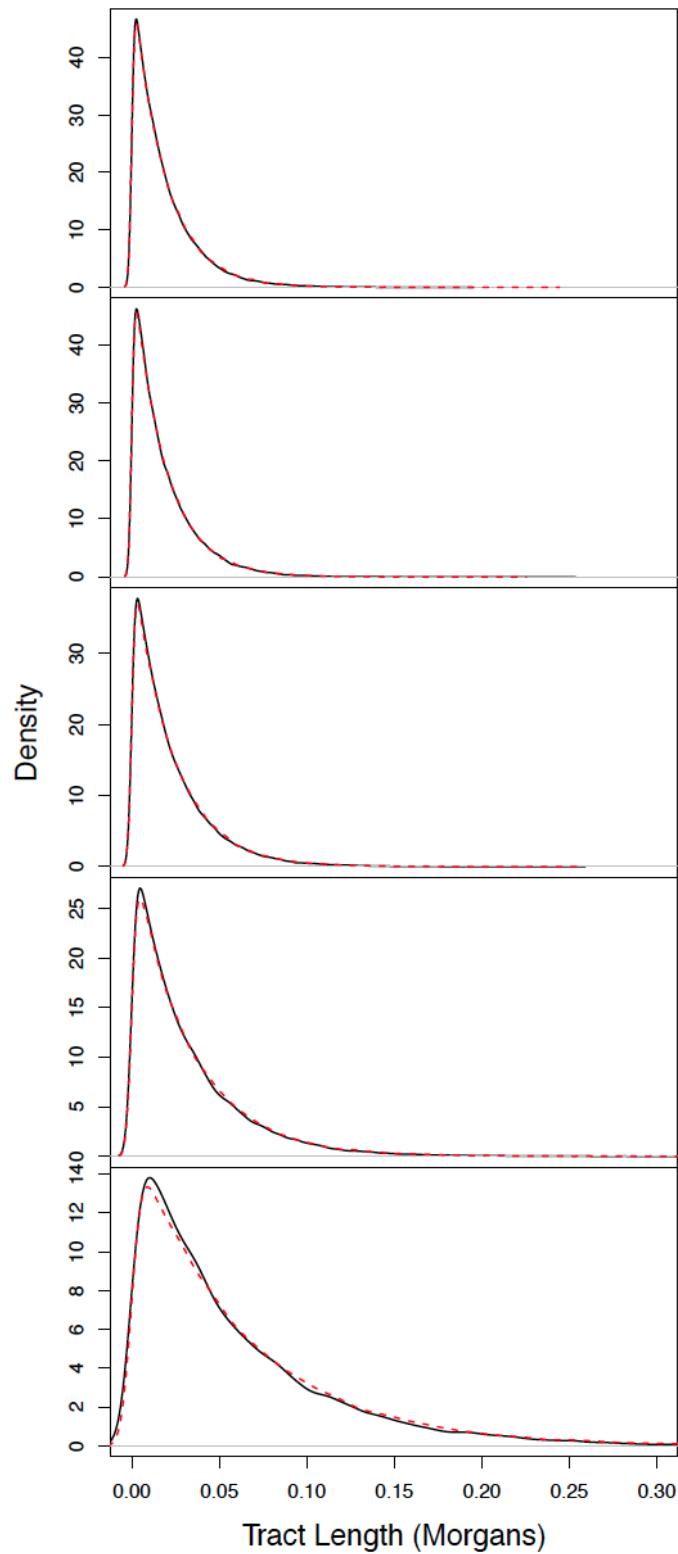
Supplementary Figure S1 Tract length distributions obtained using our tract length model approximation (solid black) and forward-in-time simulation (dashed red). In the model considered, there are five ancestry types $A_1..A_k$ and four admixture pulses occurring at 20, 40, 60, and 80 generations since the present. Each pulse in forward time contributes $\frac{1}{2}$, $\frac{1}{3}$, $\frac{1}{4}$, and $\frac{1}{5}$, respectively, of total resident genetic ancestry. Each simulation had a diploid population size of size 10,000 and we aggregated data from 50 sampled individuals across 100 simulations to produce the full tract length distribution. From top to bottom, respective ancestry tract length distributions correspond A_k, A_1, A_2, A_3, A_4.
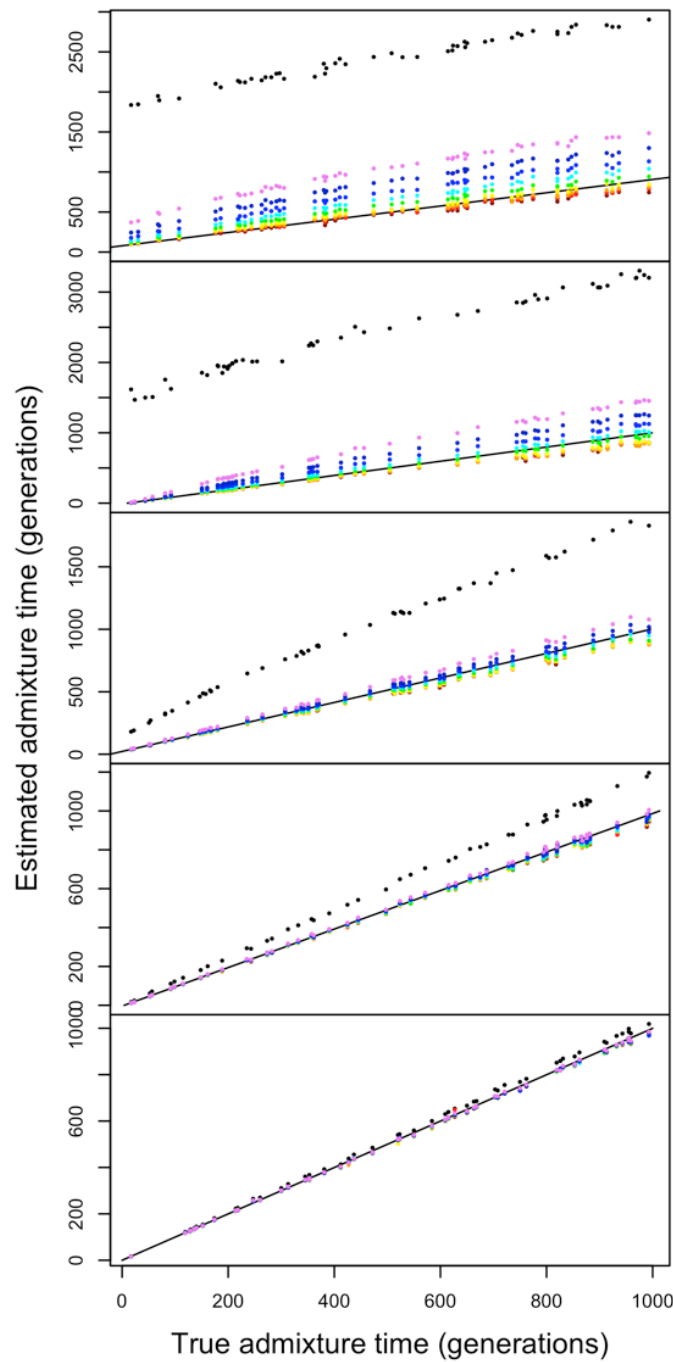
Supplementary Figure S2 Estimated admixture times for single pulse admixture models with varying levels of genetic divergence between ancestral populations. Specifically, from top to bottom, ancestral populations are 0.05, 0.1, 0.25, 0.5, and 1 N_e generations divergent from one another. LD pruned is 1 (black), 0.9 (violet), 0.8 (dark blue), 0.7 (blue), 0.6 (cyan), 0.5 (green), 0.4 (yellow), 0.3 (orange), 0.2 (red), 0.1 (dark red).
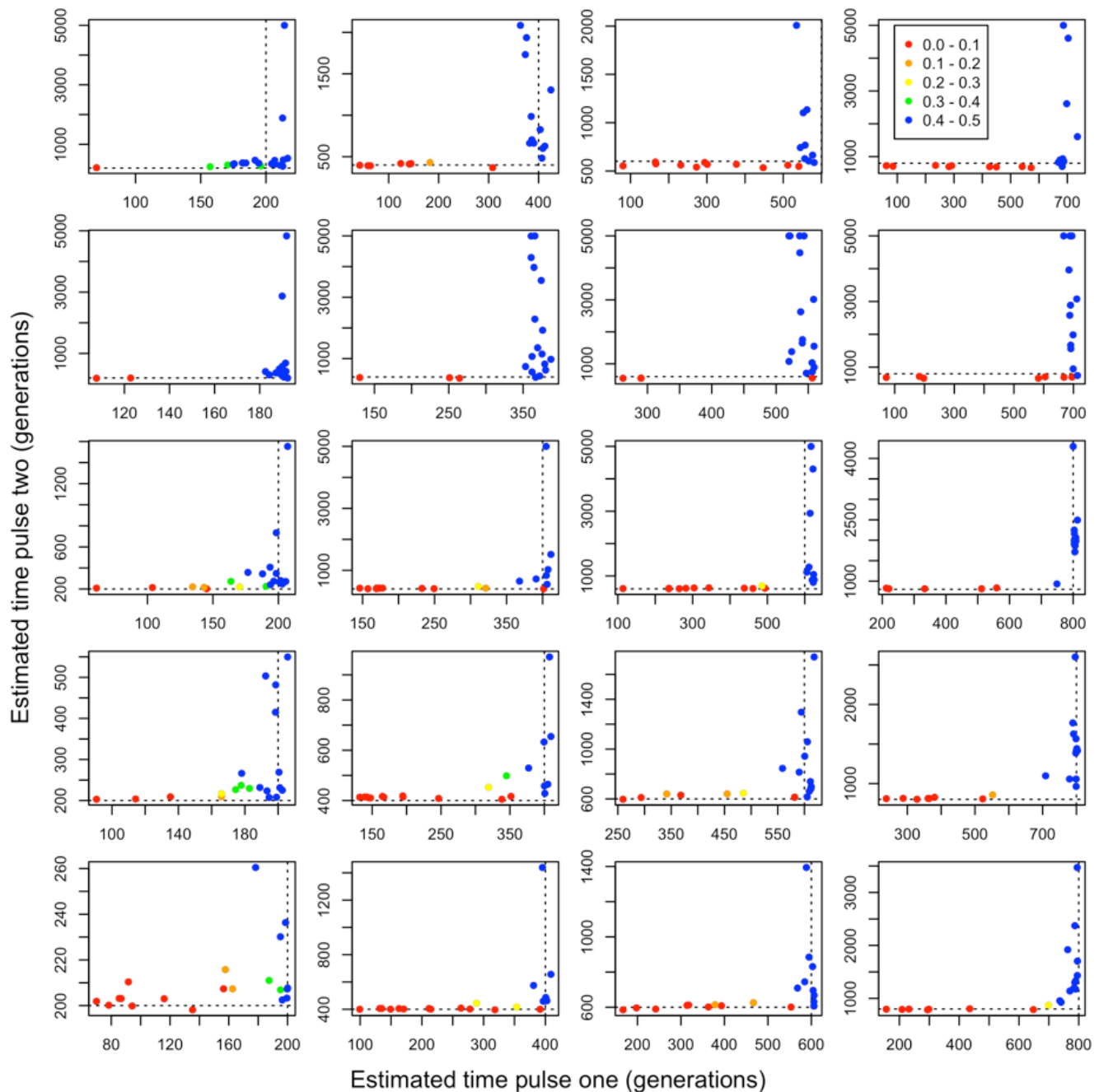
Supplementary Figure S3 Two-pulse admixture models fitted using our framework to data generated under a single pulse admixture model. We considered varying levels of population divergence. From top to bottom, the ancestral populations are 0.05, 0.1, 0.25, 0.5, and 1 N_e generation divergent from one another. From left to right, the single admixture pulse occurred 200, 400, 600, and 800 generations prior to sampling and replaced one half of the individuals in the population. Point colors correspond to the proportion of ancestry that is attributable to the second pulse with 0.0-0.1 (red), 0.1-0.2 (orange), 0.2-0.3 (yellow), 0.3-0.4 (green) and 0.4-0.5 (blue). Dashed lines reflect the true admixture time.
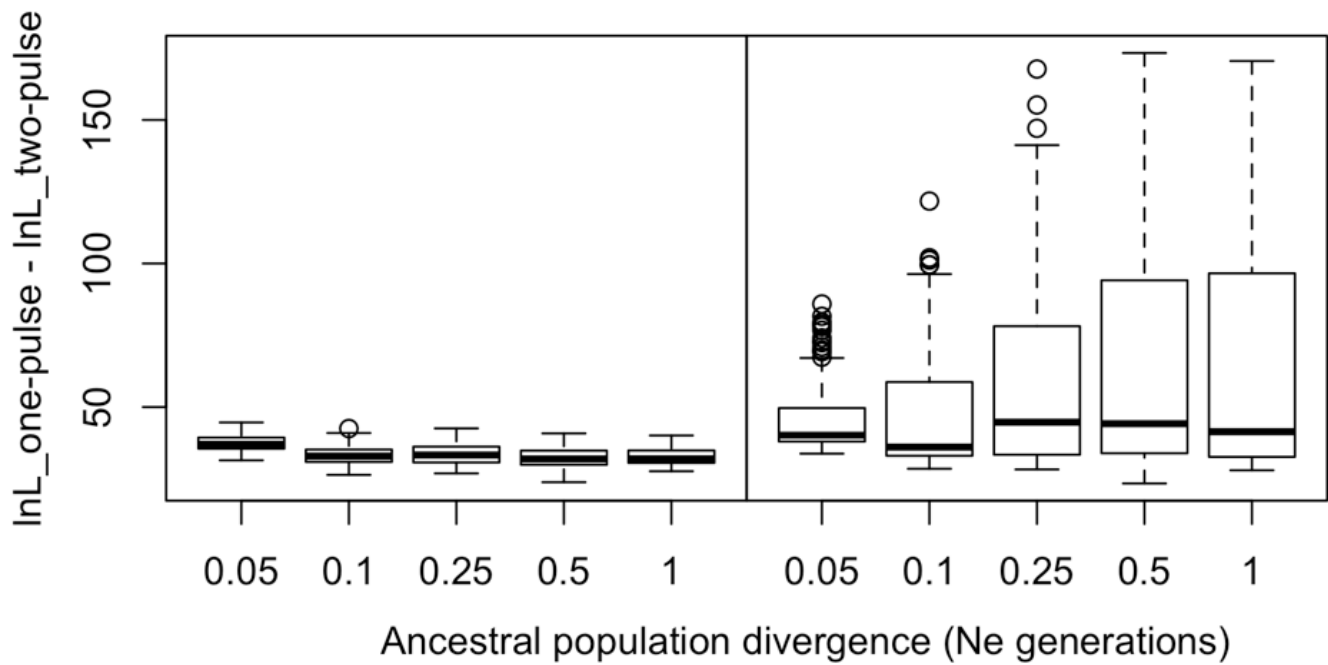
Supplementary Figure S4 The likelihood ratio between two-pulse and single-pulse ancestry models fit to data simulated under a single pulse (left) and a two pulse model (right). The single pulse model included a pulse of 50% of ancestry 50 generations prior to sampling. The two pulse model included a first pulse in forward time of 33% of ancestry 100 generations prior to sampling, and a second pulse in forward time of 25% of ancestry both from ancestry type 1, at time 20 generations prior to sampling. Each boxplot is based on 20 replicate simulations for each level of ancestral population divergence.

Table S2 Accuracy statistics of one pulse admixture model fit to two pulse admixture population.

divergence	pulse_time	mean_error	accuracy	confident_correct
0.05	20	0.0086	0.2009	0.2878
0.05	40	0.0071	0.2163	0.2383
0.05	60	0.0060	0.2302	0.1981
0.05	80	0.0053	0.2418	0.1712
0.05	200	0.0004	0.4908	0.0037
0.05	400	0.0002	0.5097	0.0023
0.05	600	0.0002	0.5249	0.001
0.05	800	0.0001	0.5341	0.0016
0.1	20	0.0080	0.0669	0.7713
0.1	40	0.0079	0.0722	0.7471
0.1	60	0.0078	0.0784	0.7221
0.1	80	0.0080	0.08362	0.7019
0.1	200	0.0046	0.3017	0.0999
0.1	400	0.0030	0.3240	0.0675
0.1	600	0.0025	0.3379	0.0525
0.1	800	0.0021	0.3496	0.0437
0.25	20	0.0010	0.00	0.9697

0.25	40	0.0011	0.0098	0.9669
0.25	60	0.001	0.0108	0.9634
0.25	80	0.0013	0.0116	0.9606
0.25	200	0.0093	0.0826	0.7203
0.25	400	0.0093	0.0894	0.6935
0.25	600	0.0092	0.0961	0.6667
0.25	800	0.0094	0.1021	0.6447
0.5	20	0.0002	0.0026	0.9912
0.5	40	0.0002	0.0028	0.9904
0.5	60	0.0003	0.0031	0.9894
0.5	80	0.0003	0.0033	0.98873
0.5	200	0.0035	0.0276	0.9088
0.5	400	0.0037	0.0304	0.8989
0.5	600	0.0039	0.0327	0.8908
0.5	800	0.0041	0.0351	0.8825
1	20	6.0757e-05	0.00070	0.99764
1	40	6.7744e-05	0.0007	0.9974
1	60	7.4457e-05	0.00084	0.99720
1	80	8.0574e-05	0.0009	0.9969
1	200	0.0008	0.0075	0.97535
1	400	0.0009	0.0082	0.97289
1	600	0.0010	0.0091	0.97002
1	800	0.0011	0.0097	0.96794

Table S3 Accuracy statistics of two pulse admixture model fit to two pulse admixture population.

divergence	pulse_time	mean_error	accuracy	confident_correct
0.05	20	0.0067	0.2022	0.2591
0.05	40	0.0062	0.2175	0.2211
0.05	60	0.0054	0.2314	0.1873
0.05	80	0.0049	0.2428	0.1631
0.05	200	0.0003	0.4907	0.0034
0.05	400	0.0002	0.5098	0.0023
0.05	600	0.0002	0.5247	0.0018
0.05	800	0.0001	0.5340	0.0016
0.1	20	0.0074	0.0667	0.7648
0.1	40	0.0077	0.0723	0.7434
0.1	60	0.0078	0.0784	0.7215
0.1	80	0.0080	0.0836	0.7016
0.1	200	0.0037	0.3021	0.0898

0.1	400	0.0029	0.3241	0.0661
0.1	600	0.0025	0.3380	0.0525
0.1	800	0.0021	0.3495	0.0438
0.25	20	0.0010	0.0090	0.9693
0.25	40	0.0011	0.0098	0.9666
0.25	60	0.0012	0.0108	0.9633
0.25	80	0.0013	0.0116	0.9604
0.25	200	0.0085	0.0825	0.7112
0.25	400	0.0090	0.0895	0.6882
0.25	600	0.0091	0.0961	0.6648
0.25	800	0.0094	0.1021	0.6440
0.5	20	0.0002	0.0026	0.9911
0.5	40	0.0002	0.0028	0.9904
0.5	60	0.0003	0.0031	0.9893
0.5	80	0.0003	0.0033	0.9886
0.5	200	0.0033	0.0276	0.9071
0.5	400	0.0036	0.0304	0.8978
0.5	600	0.0039	0.0327	0.8903
0.5	800	0.0041	0.0352	0.8823
1	20	6.0073e-05	0.0007	0.9976
1	40	6.7661e-05	0.0007	0.9974
1	60	7.4321e-05	0.0008	0.9972
1	80	8.0529e-05	0.0009	0.9969
1	200	0.0008	0.0075	0.9752
1	400	0.0009	0.0082	0.9727
1	600	0.0010	0.0091	0.9698
1	800	0.0011	0.0097	0.9679

Table S4 Accuracy statistics of two pulse admixture model fit to one pulse admixture population.

divergence	pulse_time	mean_error	accuracy	confident_correct
0.05	20	0.0073	0.0786	0.7125
0.05	40	0.0087	0.1387	0.4809
0.05	60	0.0077	0.1861	0.3124
0.05	80	0.0059	0.2214	0.2135
0.05	100	0.0047	0.2527	0.1505
0.1	20	0.0022	0.0192	0.9345
0.1	40	0.0043	0.0382	0.8655
0.1	60	0.0059	0.0570	0.8001
0.1	80	0.0075	0.0729	0.7422

0.1	100	0.0084	0.0893	0.6803
0.25	20	0.0002	0.0023	0.9921
0.25	40	0.0004	0.0048	0.9838
0.25	60	0.0007	0.0074	0.9749
0.25	80	0.0010	0.0099	0.9663
0.25	100	0.0014	0.0126	0.9576
0.5	20	5.6568e-05	0.0006	0.9976
0.5	40	0.0001	0.0014	0.9952
0.5	60	0.0001	0.0021	0.9927
0.5	80	0.0002	0.0029	0.9903
0.5	100	0.0003	0.0036	0.9877
1	20	1.4541e-05	0.0001	0.9993
1	40	3.2523e-05	0.0003	0.9987
1	60	4.7858e-05	0.0005	0.9980
1	80	6.5332e-05	0.0007	0.9974
1	100	8.6379e-05	0.0009	0.9967
0.05	200	0.0019	0.3493	0.0378
0.05	400	0.0006	0.4401	0.0081
0.05	600	0.0003	0.4881	0.0034
0.05	800	0.0002	0.5153	0.0022
0.05	1000	0.0002	0.5395	0.0015
0.1	200	0.0092	0.1532	0.4402
0.1	400	0.0059	0.2362	0.1951
0.1	600	0.0037	0.2915	0.0998
0.1	800	0.0026	0.3291	0.0602
0.1	1000	0.0018	0.3599	0.0379
0.25	200	0.0030	0.0255	0.9131
0.25	400	0.0057	0.0497	0.8301
0.25	600	0.0076	0.0715	0.7533
0.25	800	0.0090	0.0901	0.6880
0.25	1000	0.0096	0.1073	0.6260
0.5	200	0.0008	0.0075	0.9748
0.5	400	0.0017	0.0154	0.9485
0.5	600	0.0027	0.0230	0.9231
0.5	800	0.0036	0.0304	0.8986
0.5	1000	0.0043	0.0374	0.8747
1	200	0.0001	0.0020	0.9933
1	400	0.0004	0.0040	0.9865
1	600	0.0006	0.0061	0.9796
1	800	0.0009	0.0082	0.9727

| 1 | 1000 | 0.0011 | 0.0103 | 0.9657 |

Literature Cited

Begun, D. J. and C. F. Aquadro, 1993 African and north american populations of drosophila melanogaster are very different at the dna level. Nature **365**: 548.

Bergland, A. O., R. Tobler, J. Gonzalez, P. Schmidt, and D. Petrov, 2016 Secondary contact and local adaptation contribute to genome-wide patterns of clinal variation in drosophila melanogaster. Molecular ecology **25**: 1157–1174.

Bukowicki, M., S. U. Franssen, and C. Schlötterer, 2016 High rates of phasing errors in highly polymorphic species with low levels of linkage disequilibrium. Molecular ecology resources **16**: 874–882.

Caracristi, G. and C. Schlötterer, 2003 Genetic differentiation between american and european drosophila melanogaster populations could be attributed to admixture of african alleles. Molecular biology and evolution **20**: 792–799.

Chakraborty, R. and K. M. Weiss, 1988 Admixture as a tool for finding linked genes and detecting that difference from allelic association between loci. Proceedings of the National Academy of Sciences **85**: 9119–9123.

Chen, G. K., P. Marjoram, and J. D. Wall, 2009 Fast and flexible simulation of dna sequence data. Genome research **19**: 136–142.

Corbett-Detig, R. and M. Jones, 2016 Selam: simulation of epistasis and local adaptation during admixture with mate choice. Bioinformatics **32**: 3035–3037.

Corbett-Detig, R. and R. Nielsen, 2017 A hidden markov model approach for simultaneously estimating local ancestry and admixture time using next generation sequence data in samples of arbitrary ploidy. PLoS genetics **13**: e1006529.

Duchen, P., D. Živković, S. Hutter, W. Stephan, and S. Laurent, 2013 Demographic inference reveals african and european admixture in the north american drosophila melanogaster population. Genetics **193**: 291–301.

Evanno, G., S. Regnaut, and J. Goudet, 2005 Detecting the number of clusters of individuals using the software structure: a simulation study. Molecular ecology **14**: 2611–2620.

Gravel, S., 2012 Population genetics models of local ancestry. Genetics **191**: 607–619.

Gravel, S., F. Zakharia, A. Moreno-Estrada, J. K. Byrnes, M. Muzzio, *et al.*, 2013 Reconstructing native american migrations from whole-genome and whole-exome data. PLoS genetics **9**: e1004023.

Hufford, M. B., P. Lubinksy, T. Pyhäjärvi, M. T. Devengenzo, N. C. Ellstrand, *et al.*, 2013 The genomic signature of crop-wild introgression in maize. PLoS Genetics **9**: e1003477.

Kao, J. Y., A. Zubair, M. P. Salomon, S. V. Nuzhdin, and D. Campo, 2015 Population genomic analysis uncovers african and european admixture in drosophila melanogaster populations from the south-eastern united states and caribbean islands. Molecular ecology **24**: 1499–1509.

Kern, A. D. and J. Hey, 2017 Exact calculation of the joint allele frequency spectrum for isolation with migration models. Genetics **207**: 241–253.

Lachaise, D., M.-L. Cariou, J. R. David, F. Lemeunier, L. Tsacas, *et al.*, 1988 Historical biogeography of the drosophila melanogaster species subgroup. In *Evolutionary biology*, pp. 159–225, Springer.

Lachance, J. and J. R. True, 2010 X-autosome incompatibilities in drosophila melanogaster: Tests of haldane's rule and geographic patterns within species. Evolution **64**: 3035–3046.

Lack, J. B., C. M. Cardeno, M. W. Crepeau, W. Taylor, R. B. Corbett-Detig, *et al.*, 2015 The drosophila genome nexus: a population genomic resource of 623 drosophila melanogaster genomes, including 197 from a single ancestral range population. Genetics **199**: 1229–1241.

Lack, J. B., J. D. Lange, A. D. Tang, R. B. Corbett-Detig, and J. E. Pool, 2016 A thousand fly genomes: an expanded drosophila genome nexus. Molecular biology and evolution **33**: 3308–3313.

Liang, M. and R. Nielsen, 2014 The lengths of admixture tracts. Genetics **197**: 953–967.

Liang, M. and R. Nielsen, 2016 Estimating the timing of multiple admixture events using 3-locus linkage disequilibrium. bioRxiv p. 078378.

Loh, P.-R., M. Lipson, N. Patterson, P. Moorjani, J. K. Pickrell, *et al.*, 2013 Inferring admixture histories of human populations using linkage disequilibrium. Genetics **193**: 1233–1254.

Maples, B. K., S. Gravel, E. E. Kenny, and C. D. Bustamante, 2013 Rfmix: a discriminative modeling approach for rapid and robust local-ancestry inference. The American Journal of Human Genetics **93**: 278–288.

Moorjani, P., N. Patterson, J. N. Hirschhorn, A. Keinan, L. Hao, *et al.*, 2011 The history of african gene flow into southern europeans, levantines, and jews. PLoS genetics **7**: e1001373.

Nelder, J. A. and R. Mead, 1965 A simplex method for function minimization. The computer journal **7**: 308–313.

Ometto, L., S. Glinka, D. De Lorenzo, and W. Stephan, 2005 Inferring the effects of demography and selection on drosophila melanogaster populations from a chromosome-wide scan of dna variation. Molecular Biology and Evolution **22**: 2119–2130.

Paşaniuc, B., S. Sankararaman, G. Kimmel, and E. Halperin, 2009 Inference of locus-specific ancestry in closely related populations. Bioinformatics **25**: i213–i221.

Pickrell, J. K., N. Patterson, P.-R. Loh, M. Lipson, B. Berger, *et al.*, 2014 Ancient west eurasian ancestry in southern and eastern africa. Proceedings of the National Academy of Sciences **111**: 2632–2637.

Pool, J. E., 2015 The mosaic ancestry of the drosophila genetic reference panel and the d. melanogaster reference genome reveals a network of epistatic fitness interactions. Molecular biology and evolution **32**: 3236–3251.

Pool, J. E., R. B. Corbett-Detig, R. P. Sugino, K. A. Stevens, C. M. Cardeno, *et al.*, 2012 Population genomics of sub-saharan drosophila melanogaster: African diversity and non-african admixture. PLoS genetics **8**: e1003080.

Pool, J. E. and R. Nielsen, 2009 Inference of historical changes in migration rate from the lengths of migrant tracts. Genetics **181**: 711–719.

Price, A. L., A. Tandon, N. Patterson, K. C. Barnes, N. Rafaels, *et al.*, 2009 Sensitive detection of chromosomal segments of distinct

ancestry in admixed populations. PLoS genetics **5**: e1000519.

Pritchard, J. K., M. Stephens, and P. Donnelly, 2000 Inference of population structure using multilocus genotype data. Genetics **155**: 945–959.

Rieseberg, L. H., O. Raymond, D. M. Rosenthal, Z. Lai, K. Livingstone, *et al.*, 2003 Major ecological transitions in wild sunflowers facilitated by hybridization. Science **301**: 1211–1216.

Sankararaman, S., S. Mallick, M. Dannemann, K. Prüfer, J. Kelso, *et al.*, 2014 The genomic landscape of neanderthal ancestry in present-day humans. Nature **507**: 354.

Sankararaman, S., N. Patterson, H. Li, S. Pääbo, and D. Reich, 2012 The date of interbreeding between neandertals and modern humans. PLoS genetics **8**: e1002947.

Sankararaman, S., S. Sridhar, G. Kimmel, and E. Halperin, 2008 Estimating local ancestry in admixed populations. The American Journal of Human Genetics **82**: 290–303.

Skotte, L., T. S. Korneliussen, and A. Albrechtsen, 2013 Estimating individual admixture proportions from next generation sequencing data. Genetics **195**: 693–702.

Thornton, K. and P. Andolfatto, 2006 Approximate bayesian inference reveals evidence for a recent, severe bottleneck in a netherlands population of drosophila melanogaster. Genetics **172**: 1607–1619.

Ting, C.-T., A. Takahashi, and C.-I. Wu, 2001 Incipient speciation by sexual isolation in drosophila: concurrent evolution at multiple loci. Proceedings of the National Academy of Sciences **98**: 6709–6713.